

# Reconciling seismicity and geodetic locking depths on the Anza section of the San Jacinto Fault

Junle Jiang<sup>1\*</sup> and Yuri Fialko<sup>1</sup>

<sup>1</sup>Institute of Geophysics and Planetary Physics, Scripps Institution of Oceanography, University of California, San Diego, La Jolla, California, USA.

\*Corresponding author: Junle Jiang (junle@ucsd.edu)

## Key Points:

- A transition zone with heterogeneous frictional properties may explain microseismicity much below the geodetic locking depth
- Large earthquakes can penetrate beyond the geodetic locking depth to the deepest extent of seismicity, with complexity in downdip ruptures
- Our model predicts deep aseismic transients that can be potentially detected by modern geodetic techniques

This article has been accepted for publication and undergone full peer review but has not been through the copyediting, typesetting, pagination and proofreading process which may lead to differences between this version and the Version of Record. Please cite this article as doi: 10.1002/2016GL071113

## **Abstract**

Observations from the Anza section of the San Jacinto Fault in Southern California reveal that microseismicity extends to depths of 15–18 km, while the geodetically-determined locking depth is less than ~10 km. This contrasts with observations from other major faults in the region, and also with predictions of fault models assuming a simple layered distribution of frictional properties with depth. We suggest that an anomalously shallow geodetic fault locking may result from a transition zone at the bottom of seismogenic layer with spatially heterogeneous frictional properties. Numerical models of faults that incorporate stochastic heterogeneity at transitional depths successfully reproduce the observed depth relation between seismicity and geodetic locking, as well as complex spatio-temporal patterns of microseismicity with relatively scarce repeating earthquakes. Our models predict propagation of large earthquakes to the bottom of the transition zone, and ubiquitous aseismic transients below the locked zone, potentially observable using high-precision geodetic techniques.

## **1 Introduction**

Active tectonic faults commonly feature depth-dependent behavior, with recurring earthquakes and interseismic locking in the upper crust, and stable creep in the deeper mostly aseismic substrate. The transition between the upper locked and lower creeping regions is particularly important for understanding fault behavior and earthquake physics, due to its crucial role in the earthquake nucleation [*Das and Scholz, 1983; Lapusta and Rice, 2003*] and arrest [*Jiang and Lapusta, 2016*]. The depth extent of fault locking can be estimated independently using seismic and geodetic observations. A systematic comparison of the depth limit of microseismicity and fault locking depths inferred from inversions of geodetic data reveals a general agreement between the seismic and geodetic locking depths for many active

faults in Southern California [*Smith-Konter et al.*, 2011]. Among a few notable exceptions is the Anza section of the San Jacinto Fault [e.g., *Smith-Konter et al.*, 2011; *Lindsey et al.*, 2014].

The San Jacinto Fault (SJF) is historically the most seismically active fault in Southern California, with 9 major earthquakes (magnitude M 6–7) over the past 120 years, in sharp contrast with the nearby quiescent Southern San Andreas Fault (SAF). The fault segment near Anza has not ruptured for more than 200 years [*Rockwell et al.*, 2006], and is considered to represent a “seismic gap,” posing a regional seismic hazard [*Thatcher et al.*, 1975; *Sanders and Kanamori*, 1984]. On other parts of the fault, microseismicity (M 2–4) is observed to predominantly occur at depths of 10–18 km, with lateral variations in maximum hypocenter depth ranging from 14 to 18 km, which follows the regional trend of surface heat flow [*Sanders*, 1990; *Hauksson et al.*, 2012; Fig. 1].

Geodetic observations of interseismic strain accumulation across the Anza section of the San Jacinto Fault (SJF) revealed a high shear strain rate and an anomalously shallow locking depth. Based on the trilateration data, *Lisowski et al.* [1991] inferred a locking depth of just 5 to 6 km assuming a homogeneous elastic model, significantly shallower than the depths of seismicity, and proposed that such a discrepancy could be due to a compliant fault zone with a significantly reduced shear modulus, but could not rule out alternatives such as fault creep, which might affect the near-field measurements. *Lindsey et al.* [2014] tested both hypotheses using an updated set of GPS velocities (including new campaign data collected in 2014–2015) and InSAR observations; they were able to rule out the localized shallow fault creep above a rate of 0.2 mm/yr.

Inversions of available geodetic data assuming a homogeneous elastic half space produce fault slip rates [*Lindsey et al.*, 2014] that are in excellent agreement with geologic estimates [*Rockwell et al.*, 1990; *Petersen and Wesnousky*, 1994; *van der Woerd et al.*, 2006;

*Oskin et al.*, 2007; *Behr et al.*, 2010]. The best-fitting SAF locking depth,  $10.3 \pm 1.6$  km, is comparable to the depth of seismicity on that fault. The inferred SJF locking depth of  $7.7 \pm 1.0$  km is in a good agreement with previous geodetic models of the area [*Lisowski et al.*, 1991; *Becker et al.*, 2005; *Lundgren et al.*, 2009; *Platt and Becker*, 2010], but is much smaller than the observed depth extent of seismicity. The consideration of a heterogeneous elastic structure, including a compliant fault zone constrained by seismic tomography [*Allam and Ben-Zion*, 2012], increases the inferred SJF locking depth to  $10.4 \pm 1.3$  km, which is still much smaller than the 14–18 km maximum depth of seismicity near Anza (Fig. 1). Reconciling the geodetically inferred locking depth with the depth distribution of seismicity would require reductions in fault zone rigidity that are much larger than those constrained by seismic tomography [*Allam and Ben-Zion*, 2012]. Alternatively, this discrepancy could be at least partially attributed to distributed plastic yielding in the fault zone in the interseismic period [*Lindsey et al.*, 2014]. *Wdowinski* [2009] proposed that deeper parts of the seismogenic region beneath Anza undergo “brittle creep,” such that the same region exhibits both stable and unstable slip. While laboratory observations of the rate dependence of friction preclude a possibility that the same material can creep and nucleate slip instabilities, it is possible that creep may trigger microseismicity in the transition zone between the fault regions associated with unstable (velocity-weakening, VW) and stable (velocity-strengthening, VS) frictional properties [*Lapusta and Rice*, 2003]. The bulk of the transition zone may remain stable until conditions for nucleation of a large rupture are met [*Ruina*, 1983; *Scholz*, 1998]. If the depth of microseismicity is not indicative of fault locking — e.g., in the presence of isolated VW patches surrounded by VS areas — one might expect the resulting microseismicity to be dominated by repeating earthquakes, as observed on the creeping section of the SAF north of Parkfield [e.g. *Nadeau and Johnson*, 1998; *Sammis and Rice*, 2001]. However, the repeating earthquakes at the bottom of the seismogenic zone on the SJF appear to account for only a

small fraction of the earthquake catalog (*T. Taira and R. Burgmann*, personal communication in *Lindsey et al.*, 2014).

## **2 Physical relation between seismicity and geodetic fault locking**

The discrepancy between the shallower geodetic locking depth and greater depths of seismicity for the Anza section is particularly at odds with predictions of fault models with conventional assumptions on rheological transitions with depth (Fig. 2). Models with stress-controlled slip on the fault interface [*Savage*, 2006] showed that slip rates below the fully locked region gradually increase downdip, rather than stay uniform at the plate rate as commonly assumed in conventional dislocation models [*Savage and Burford*, 1973]. The geodetically-determined locking depth, typically based on the elastic dislocation model, can thus be substantially deeper than the bottom of the locked zone. *Jiang and Lapusta* [2015] explored how the depths of microseismicity and geodetic fault locking are related in friction-based fault models with typical depth variations in rate-and-state frictional properties [*Blanpied*, 1995] and different depth limits for dynamic fault weakening (illustrated in Fig. 2B). They confirmed that the transition from effectively locked zones to fully creeping zones can occur over a broad depth range. Furthermore, the effective locking depth, near the top of the locked-creeping transition zone, is closely associated with concentrated loading that promotes seismicity at the bottom of the seismogenic zone. Over the post- and inter-seismic period, the effective locking depth either stays in place or becomes shallower due to the updip migration of loading fronts [*Jiang and Lapusta*, 2016], while the geodetic locking depth typically increases with time due to postseismic slip expanding in space and decaying in amplitude in the deeper creeping VS region—a process similar to the “stress shadowing” effect [e.g., *Burgmann et al.*, 2005; *Hetland and Simons*, 2010]. For that reason, the geodetic

locking depth is expected to be close to, or deeper than the depth extent of seismicity toward the end of the interseismic period. These conclusions appear to be consistent with the observations available for the Carrizo, Coachella, and Mojave segments on the SAF [Smith-Konter *et al.*, 2011], but fail to explain observations from the Anza section of the SJF.

Here we propose that a transition zone that spans a broad depth range with highly heterogeneous frictional properties may explain the discrepancy between seismic and geodetic observations from the Anza section (Fig. 2C). The existence of such a broad transition zone effectively invalidates the commonly-held assumption that the rheological boundary (the VW/VS transition or the depth limit of enhanced dynamic weakening) is relatively sharp and variations in material properties along-strike can be negligible compared to variations in depth [e.g., Scholz, 1998]. In this study, we explore to what extent models of faults with spatially heterogeneous frictional properties can reconcile the seismic and geodetic observations, and further study the implications of such models for the behavior of large earthquakes and interseismic deformation.

### **3 Models of faults with heterogeneous frictional properties**

We developed 3D models of faults governed by laboratory friction laws and spatially heterogeneous fault properties to explore the relation between seismicity and fault locking depth that is potentially relevant to the Anza section (Fig. 3). A quintessential ingredient in our models is the rate- and state-dependent friction laws [Dieterich, 1979, 1981; Ruina, 1983], formulated based on laboratory experiments at slip rates appropriate for earthquake nucleation ( $10^{-9}$  to  $10^{-3}$  m/s). Such laws allow one to interpret the seismogenic zones as areas of velocity-weakening properties that support earthquake initiation and rupture, and the other fault areas as having velocity-strengthening properties that promote stable creep. Models with

the rate-and-state friction have reproduced a wide range of fault behaviors including earthquake sequences and aseismic slip [Dieterich, 1992; Lapusta et al., 2000; Kaneko and Lapusta, 2008; Kaneko and Fialko, 2011; Barbot et al., 2012; Kaneko et al., 2013; Lindsey and Fialko, 2016].

Unlike in the commonly assumed case of piece-wise linear variations in the rate-and-state parameters with depth [e.g., Scholz, 1998], the rheological transition in our fault models is represented by stochastic heterogeneity in rate-and-state frictional properties over a broad depth range (8–15 km) between the shallower VW region (0–8 km) and the deeper VS region (>15 km) (Fig. 3A). The broad and heterogeneous transition zone may be due to spatially variable lithology and/or pore pressure [e.g., Mitchell et al., 2016], or due to effective mechanical heterogeneity that results from the complex structure of the relatively immature San Jacinto Fault Zone. Stochastic characterization of certain physical properties—e.g., coseismic slip distribution [Mai and Beroza, 2002], prestress field [Ripperger et al., 2007], and fault roughness [Dunham et al., 2011; Shi et al., 2013]—were previously used to understand and reproduce the randomness in earthquake rupture scenarios. In the same spirit, we adopt a stochastic description of the rate-and-state parameter ( $a - b$ ) by a Gaussian autocorrelation function with a correlation length of 800 m to introduce greater variability in the simulated fault behavior within the transition zone. The model we present here is based on a random realization of fault property distributions, in which several areas within the transition zone are of sizes larger than the local nucleation zone sizes based on theoretical estimates [Rice and Ruina, 1983; Ampuero and Rubin, 2008; Chen and Lapusta, 2009] (see details in Supplementary Information; Fig. S1). The background frictional properties are based on typical laboratory values [Blanpied, 1995]. All parameters of the model are listed in Table S1.

The long-term behavior of a fault in such a model is explored with a spectral boundary integral method [Lapusta and Liu, 2009; based on Dieterich, 1979, 1981; Ruina, 1983; Geubelle and Rice, 1995; Ben-Zion and Rice, 1997; Lapusta et al., 2000]. The methodology is computationally challenging but resolves all stages of fault slip, including the spontaneous nucleation and fully dynamic rupture of small and large earthquakes, postseismic transients, and interseismic creep.

### **3 Results and discussion**

#### **3.1 Reproducing deeper seismicity and shallower geodetic locking**

The simulated fault behavior is characterized by robust microseismicity in the interseismic periods between occasional large (moment magnitude 6.7–6.9) events (Fig. 3B). Microseismicity is typically accompanied by aseismic slip that surrounds the ruptured region and sometimes triggers aseismic transients that propagate over larger distances (Fig. 3B(iv)). Spontaneous aseismic transients also occur in the transition zone as failed attempts of nucleation in VW regions. These aseismic transients sometimes precede the nucleation of large earthquakes (Fig. 3B(i)). Almost always, these large events rupture through the upper seismogenic region and the entire transition zone (Fig. 3B(ii)), followed later by postseismic slip and resumption of microseismicity (Fig. 3B(iii)).

Fig. 3C depicts the spatial distribution of slip during a typical large earthquake and the locations and equivalent rupture sizes of microseismicity (based on a circular crack model [Eshelby, 1957] with an assumed static stress drop of 3 MPa) in our model. The large event is spatially extensive, with a peak coseismic slip of less than 2 m at shallower depths, tapering to zero at greater depths, while the microseismicity occurs within the transition zone. The occurrence of these large events is quasi-periodic, with an average slip of ~2 m and a mean



recurrence interval of ~100 years, which are reasonably close to the average surface slip (2.5–2.9 m) estimated from geomorphic offsets [Salisbury *et al.*, 2012] and paleoseismic estimates of recurrence intervals ( $254 \pm 120$  yr) [Rockwell *et al.*, 2014] within their respective uncertainties.

Small earthquakes in the model follow several different patterns. In rather isolated VW regions, micro-earthquakes are mostly repeating events. In more interconnected VW regions, seismicity occurs with greater variability in the event locations and sizes so that the respective events are unlikely to be identified as repeating earthquakes. A large portion of the transition zone does not produce seismic activity due to VS properties, or VW properties in areas smaller than the critical nucleation zone. The variability observed in simulated earthquakes implies that a stochastic form of heterogeneity is more plausible for the Anza section than a highly-organized structure, e.g., abundant VW patches surrounded by VS regions, because the latter model would predominantly produce repeating earthquakes [Chen and Lapusta, 2009], which are not commonly observed in the region (T. Taira and R. Burgmann, personal communication in Lindsey *et al.*, 2014). Overall, approximately 36% of the transition zone experiences seismic failure during small earthquakes, while VW regions account for 75% of the entire zone in our model, suggesting that most VW regions slip aseismically in the interseismic period.

We infer the geodetic locking depth, together with the plate loading rate, based on a fault-normal profile of the along-strike surface velocity that results from fault slip rates averaged over 5 years in our model (Fig. 4). To avoid the influence of creep near the surface and from the VS regions that bound the model along strike, we only consider the depth profile of average fault slip rates through the mid-point of the fault (Fig. 4A), assuming a fully locked fault at depths shallower than 5 km (Fig. 4B), and calculate the surface velocity as in a 2D problem (Fig. 4D). The surface velocity is calculated at stations with a spacing that

increases from 5 km near the fault to 15 km in the far field (300 km away), assuming uncorrelated Gaussian noises decreasing from 1.5 to 0.5 mm/yr, in order to better resolve large variations in the signal around the fault, as well as the far-field velocity. We then invert for the geodetic locking depths using an analytic solution for a semi-infinite screw dislocation in a homogeneous elastic half space [Savage and Burford, 1973], in a Bayesian formulation [Bayes and Price, 1763], with minimal *a priori* constraints on the plate loading rate and locking depth (sufficiently broad uniform prior distributions). We perform inversions using synthetic data from multiple time windows throughout the earthquake cycles excluding large events ( $M_w > 6$ ) (Fig. 4C). For one late-interseismic time window, the inferred plate loading rate is  $16.3 \pm 0.5$  mm/yr from its posterior distribution (Fig. 4E), recovering the true rate of  $\sim 15.8$  mm/yr in our model within assumed uncertainties. The inferred geodetic locking depth is  $9.0 \pm 2.0$  km, shallower than the depth range of 10–15 km for the microseismicity in the model, thus successfully reproducing the observed depth relation of seismicity and geodetic fault locking on the Anza section. A decrease in geodetic locking depths toward the end of the cycle in our model is mainly due to aseismic transients and afterslip associated with microseismicity in the transition zone. When averaged over time intervals of the order of years, regions below the seismogenic zone still have higher slip rates compared to those produced in models that assume sharp transitions of frictional properties (Fig. 4B), which reduces the effective geodetic locking depth.

To this end, our model demonstrates a plausible scenario in which faults can have a shallow geodetic locking depth and a deeper extent of seismicity. The key to reproducing such a relation is a transition zone with spatially heterogeneous rate-dependence of friction. The model can be further tailored to explain additional aspects of observations from the Anza section such as along-strike variations in seismic productivity and the depth extent of seismicity (Fig. 1), variability in coseismic slip [Salisbury, 2012; Rockwell *et al.*, 2014], etc.

While such detailed simulations will involve additional assumptions and are beyond the scope of this study, we note that they would unlikely change the main results presented above.

### **3.2 Implications for coseismic and interseismic phenomena**

Our results suggest that the main features in current seismic and geodetic observations for the Anza section can be explained by fault models based on quasi-static rate-and-state friction alone, without resorting to the enhanced dynamic weakening at high slip rates ( $>0.1$  m/s), which is amply documented in recent high-speed laboratory experiments [*Di Toro et al.*, 2011; *Brown and Fialko*, 2012; *Tullis*, 2015, and references therein] and supported by theoretical studies [*Rice*, 2006]. It is likely that geometrical and structural complexities of the relatively immature San Jacinto Fault incur additional resistance during dynamic slip and limit the extent of coseismic weakening [*Fang and Dunham*, 2013]. This possibility alludes to mechanical differences between the San Jacinto Fault and more mature faults like the San Andreas Fault, where enhanced weakening during earthquakes is inferred from interpretations of seismic quiescence being a result of deeper-penetrating earthquake ruptures [*Jiang and Lapusta*, 2016] and is consistent with the operation of faults at low stress levels [*Noda et al.*, 2011].

The behavior of large earthquakes in our models is of great interest, since it may be relevant to assessments of the regional seismic hazard. The depth extent of large earthquakes clearly exceeds the geodetic locking depth of  $\sim 10$  km in our models (Fig. 3). This relation is contrary to the conclusion of *Jiang and Lapusta* [2015] based on models that consider simpler rheological transitions and typical co-, post- and inter-seismic partitioning of fault slip. Although coseismic slip is tapered toward greater depths, the deeper rupture fronts

present more complexities than the shallower counterparts, due to the heterogeneous stress field and coseismic weakening potential in the transition zone (Fig. S2). These complex features in the dynamic rupture might contribute to generating enhanced high-frequency radiation at the downdip end of seismic ruptures, as has been documented for some earthquakes on thrust faults [e.g., *Avouac et al.*, 2015].

Observations of seismicity and deformation due to the San Jacinto Fault suggest that some triggered aseismic transients likely occur on the deeper part of the fault [*Inbal et al.*, 2014]. In our models, aseismic transients sometimes occur in the transition zone, in the form of spontaneous or triggered transients, or postseismic slip following microseismicity. These aseismic slip events occasionally interact with small and large earthquakes (Fig. 3). Profiles of surface displacements near the fault over the post- and inter-seismic periods (Fig. S3) show that microseismicity and associated aseismic transients can produce spatially coherent signals over time scales of years and less in the east and vertical components of the velocity field, while the north component largely reflects secular trends of surface velocity. Our simulations thus suggest that variations in fault slip at the bottom of the seismogenic zone may be potentially detectable and verifiable by modern geodetic techniques with sufficient spatial and temporal resolution.

#### **4 Conclusions**

We propose that a broad, heterogeneous transition zone below the nominally locked seismogenic zone may explain the apparent discrepancy between the shallow geodetic locking depth and deeper extent of seismicity on the Anza section of the San Jacinto Fault. Our models of faults with stochastic heterogeneity in frictional properties successfully reproduce such a depth relation between seismic and geodetic estimates, as well as the

scarcity of repeating micro-events in the region. The developed models may also aid assessments of regional seismic hazard due to large events and guide future observational efforts in exploring aseismic transient phenomena associated with seismogenic faults.

### **Acknowledgments**

This study was supported by a grant from the Southern California Earthquake Center (SCEC, funded by NSF Cooperative agreement EAR-0529922 and USGS Cooperative agreement 07HQAG0008). This is SCEC contribution no. 6376. J. J. was supported by a Green Foundation Postdoctoral Fellowship in the Institute of Geophysics and Planetary Physics, Scripps Institution of Oceanography, University of California, San Diego. Numerical data are available from the authors upon request.

## References

- Allam, A. A., and Y. Ben-Zion (2012), Seismic velocity structures in the southern California plate-boundary environment from double-difference tomography, *Geophys. J. Int.*, 190(2), 1181–1196, doi:10.1111/j.1365-246X.2012.05544.x.
- Ampuero, J.-P., and A. M. Rubin (2008), Earthquake nucleation on rate and state faults—Aging and slip laws, *J. Geophys. Res. Solid Earth*, 113(B1).
- Avouac, J.-P., L. Meng, S. Wei, T. Wang, and J.-P. Ampuero (2015), Lower edge of locked Main Himalayan Thrust unzipped by the 2015 Gorkha earthquake, *Nature Geosci*, 8(9), 708–711.
- Barbot, S., N. Lapusta, and J.-P. Avouac (2012), Under the hood of the earthquake machine: Toward predictive modeling of the seismic cycle, *Science*, 336 (6082), 707–710, doi:10.1126/science.1218796.
- Bayes, M., and M. Price (1763), An essay towards solving a problem in the doctrine of chances. by the late rev. Mr. Bayes, F. R. S. communicated by Mr. Price, in a letter to John Canton, A. M. F. R. S., *Philosophical Transactions*, 53, 370–418, doi:10.1098/rstl.1763.0053.
- Becker, T. W., J. L. Hardebeck, and G. Anderson (2005), Constraints on fault slip rates of the southern California plate boundary from GPS velocity and stress inversions, *Geophys. J. Int.*, 160 (2), 634–650, doi:10.1111/j.1365-246X.2004.02528.x.
- Behr, W., D. Rood, K. Fletcher, N. Guzman, R. Finkel, T. Hanks, K. Hudnut, K. Kendrick, J. Platt, W. Sharp, R. Weldon, and J. Yule (2010), Uncertainties in slip-rate estimates for the Mission Creek strand of the Southern San Andreas Fault at Biskra Palms Oasis, Southern California, *GSA Bulletin*, 122(9-10), 1360–1377, doi:10.1130/B30020.1.

- Ben-Zion, Y., and J. R. Rice (1997), Dynamic simulations of slip on a smooth fault in an elastic solid, *J. Geophys. Res.*, 102(B8), 17771–17784, doi:10.1029/97JB01341.
- Blanpied, M. L., D. A. Lockner, and J. D. Byerlee (1995), Frictional slip of granite at hydrothermal conditions, *J. Geophys. Res. Solid Earth*, 100 (B7), 13,045–13,064.
- Brown, K. M., and Y. Fialko (2012), “melt welt” mechanism of extreme weakening of gabbro at seismic slip rates, *Nature*, 488 (7413), 638–641.
- Burgmann, R., M. G. Kogan, G. M. Steblov, G. Hilley, V. E. Levin, and E. Apel (2005), Interseismic coupling and asperity distribution along the Kamchatka subduction zone, *J. Geophys. Res. Solid Earth*, 110, B07405, doi: 10.1029/2005JB003648.
- Chen, T., and N. Lapusta (2009), Scaling of small repeating earthquakes explained by interaction of seismic and aseismic slip in a rate and state fault model, *J. Geophys. Res.*, 114, B01311, doi:10.1029/2008JB005749.
- Das, S., and C. H. Scholz (1983), Why large earthquakes do not nucleate at shallow depths, *Nature*, 141(3), 183–206, doi:10.1016/j.pepi.2003.11.002.
- Day, S. M., L. A. Dalguer, and N. Lapusta (2005), Comparison of finite difference and boundary integral solutions to three-dimensional spontaneous rupture. *J. Geophys. Res.* 110, B12307.
- Di Toro, G., R. Han, T. Hirose, N. De Paola, S. Nielsen, K. Mizoguchi, F. Ferri, M. Cocco, and T. Shimamoto (2011), Fault lubrication during earthquakes, *Nature*, 471(7339), 494–498, doi:10.1038/nature09838.
- Dieterich, J. H. (1979), Modeling of rock friction .1. Experimental results and constitutive equations, *J. Geophys. Res.*, 84 (NB5), 2161–2168, doi:10.1029/JB084iB05p02161.

- Dieterich, J. H. (1981), Potential for geophysical experiments in large scale tests, *Geophys. Res. Lett.*, 8(7), 653–656, doi:10.1029/GL008i007p00653/pdf.
- Dieterich, J. H. (1992), Earthquake nucleation on faults with rate- and state-dependent strength, *Tectonophysics*, 211(1), 115–134, doi: [http://dx.doi.org/10.1016/0040-1951\(92\)90055-B](http://dx.doi.org/10.1016/0040-1951(92)90055-B).
- Doser, D. I., and H. Kanamori (1986), Depth of seismicity in the Imperial Valley region (1977-1983) and its relationship to heat flow, crustal structure, and the October 15, 1979, earthquake, *J. Geophys. Res.*, 91, 675–688.
- Dunham, E. M., D. Belanger, L. Cong, and J. E. Kozdon (2011), Earthquake ruptures with strongly rate-weakening friction and off-fault plasticity, part 2: Nonplanar faults, *Bull. Seismol. Soc. Am.*, 101(5), 2308–2322, doi: 10.1785/0120100076.
- Eshelby, J. D. (1957), The Determination of the elastic field of an ellipsoidal inclusion, and related problems, *Proc. R. Soc. Lond. A*, 241(1226), 376-396; DOI: 10.1098/rspa.1957.0133.
- Fang, Z., and E. M. Dunham (2013), Additional shear resistance from fault roughness and stress levels on geometrically complex faults, *J. Geophys. Res. Solid Earth*, 118 (7), 3642–3654, doi:10.1002/jgrb.50262.
- Geubelle, P. H., and J. R. Rice (1995), A spectral method for three-dimensional elastodynamic fracture problems, *Journal Of The Mechanics And Physics Of Solids*, 43 (11), 1791–1824.
- Hauksson, E., W. Yang, and P. M. Shearer (2012), Waveform relocated earthquake catalog for Southern California (1981 to June 2011), *Bull. Seismol. Soc. Am.*, 102(5), 2239–2244, doi:10.1785/0120120010.



- Hetland, E. A., and M. Simons (2010), Post-seismic and interseismic fault creep II: transient creep and interseismic stress shadows on megathrusts, *Geophys. J. Int.*, 181(1), 99–112, doi:10.1111/j.1365-246X.2009.04482.x.
- Inbal, A., J. P. Avouac, and J. P. Ampuero (2014), Seismic and Aseismic Slip on the San-Jacinto Fault Near Anza, CA, from Joint Analysis of Strain and Aftershock Data, 2014 AGU Fall Meeting Abstracts.
- Jiang, J., and N. Lapusta (2015), Connecting depths of seismicity, fault locking, and coseismic slip using long-term fault models, 2015 AGU Fall Meeting Abstracts.
- Jiang, J., and N. Lapusta (2016), Deeper penetration of large earthquakes on seismically quiescent faults, *Science*, 352(6291), 1293–1297, doi:10.1126/science.aaf1496.
- Kaneko, Y., and Y. Fialko (2011), Shallow slip deficit due to large strike-slip earthquakes in dynamic rupture simulations with elasto-plastic off-fault response, *Geophys. J. Int.*, 186(3), 1389–1403, doi:10.1111/j.1365-246X.2011.05117.x.
- Kaneko, Y., and N. Lapusta (2008), Variability of earthquake nucleation in continuum models of rate-and-state faults and implications for aftershock rates, *J. Geophys. Res. Solid Earth*, 113, B12312, doi:10.1029/2007JB005154.
- Kaneko, Y., Y. Fialko, D. Sandwell, X. Tong and M. Furuya (2013), Interseismic deformation and creep along the central section of the North Anatolian fault (Turkey): InSAR observations and implications for rate-and-state friction properties, *J. Geophys. Res.*, 118, 689-697.
- Lachenbruch, A. H., and J. H. Sass (1980), Heat flow and energetics of the San Andreas fault zone, *J. Geophys. Res. Solid Earth*, 85(B11), 6185–6222, doi:10.1029/JB085iB11p06185.

- Lapusta, N., and Y. Liu (2009), Three-dimensional boundary integral modeling of spontaneous earthquake sequences and aseismic slip, *J. Geophys. Res. Solid Earth*, 114 (B9), doi:10.1029/2008JB005934.
- Lapusta, N., and J. R. Rice (2003), Nucleation and early seismic propagation of small and large events in a crustal earthquake model, *J. Geophys. Res. Solid Earth*, 108(B4), n/a–n/a, doi:10.1029/2001JB000793, 2205.
- Lapusta, N., J. R. Rice, Y. Ben-Zion, and G. T. Zheng (2000), Elastodynamic analysis for slow tectonic loading with spontaneous rupture episodes on faults with rate- and state-dependent friction, *J. Geophys. Res. Solid Earth*, 105(B10), 23,765–23,789, doi:10.1029/2000JB900250.
- Lindsey, E. O., and Y. Fialko (2016), Geodetic constraints on frictional properties and earthquake hazard in the Imperial Valley, Southern California, *J. Geophys. Res. Solid Earth*, 121 (2), 1097–1113, doi:10.1002/2015JB012516, 2015JB012516.
- Lindsey, E. O., V. J. Sahakian, Y. Fialko, Y. Bock, S. Barbot, and T. K. Rockwell (2014), Interseismic strain localization in the San Jacinto fault zone, *Pure. Appl. Geophys.*, 171, 2937–2954, doi:10.1007/s00024-013-0753-z.
- Lisowski, M., J. C. Savage, and W. H. Prescott (1991), The velocity field along the San Andreas fault in Central and Southern California, *J. Geophys. Res. Solid Earth* (1978–2012), 96(B5), 8369–8389, doi:10.1029/91JB00199.
- Lundgren, P., E. A. Hetland, Z. Liu, and E. J. Fielding (2009), Southern San Andreas-San Jacinto fault system slip rates estimated from earthquake cycle models constrained by GPS and interferometric synthetic aperture radar observations, *J. Geophys. Res. Solid Earth*, 114 (B2), n/a–n/a, doi:10.1029/2008JB005996, b02403.

- Mai, P. M., and G. C. Beroza (2002), A spatial random field model to characterize complexity in earthquake slip, *J. Geophys. Res.*, 107 (10.1029), 2001.
- Mitchell, E. K., Y. Fialko, and K. M. Brown (2016), Velocity-weakening behavior of Westerly granite at temperature up to 600 °C, *J. Geophys. Res. Solid Earth*, 121, doi:10.1002/2016JB013081.
- Nadeau, R. M., and L. R. Johnson (1998), Seismological studies at Parkfield vi: Moment release rates and estimates of source parameters for small repeating earthquakes, *Bull. Seismol. Soc. Am.*, 88(3), 790–814.
- Noda, H., and N. Lapusta (2010), Three-dimensional earthquake sequence simulations with evolving temperature and pore pressure due to shear heating: Effect of heterogeneous hydraulic diffusivity, *J. Geophys. Res.*, 115(B12), doi:10.1029/2010JB007780.
- Noda, H., and N. Lapusta (2013), Stable creeping fault segments can become destructive as a result of dynamic weakening, *Nature*, 493(7433), 518–521, doi: 10.1038/nature11703.
- Noda, H., N. Lapusta, and J. R. Rice (2011), Earthquake Sequence Calculations with Dynamic Weakening Mechanisms: Statically Strong but Dynamically Weak Fault and Low Interseismic Shear Stress, *Multiscale and Multiphysics Processes in Geomechanics*, pp. 149–152.
- Oskin, M., L. Perg, D. Blumentritt, S. Mukhopadhyay, and A. Iriondo (2007), Slip rate of the Calico Fault: Implications for geologic versus geodetic rate discrepancy in the Eastern California Shear Zone, *J. Geophys. Res. Solid Earth*, 112, B03402, doi:10.1029/2006JB004451.
- Palmer, A., and J. R. Rice (1973), The growth of slip surfaces in the progressive failure of over-consolidated clay, *Proc. R. Soc. Lond. A* 332, 1591, 527-548.

- Petersen, M. D., and S. G. Wesnousky (1994), Fault slip rates and earthquake histories for active faults in Southern California, *Bull. Seismol. Soc. Am.*, 84(5), 1608–1649.
- Platt, J. P., and T. W. Becker (2010), Where is the real transform boundary in California? *Geochem. Geophys. Geosyst.*, 11, Q06012, doi:10.1029/2010GC003060.
- Plesch, A., J. Shaw, C. Benson, W. A. Bryant, S. Carena, M. Cooke, J. F. Dolan, G. Fuis, E. Gath, L. Grant, E. Hauksson, T. H. Jordan, M. Kamerling, M. Legg, S. Lindvall, H. Magistrale, C. Nicholson, N. Niemi, M. E. Oskin, S. Perry, G. Planansky, T. Rockwell, P. M. Shearer, C. Sorlien, M. P. Suss, J. Suppe, J. Treiman, and R. Yeats (2007), Community Fault Model (CFM) for Southern California, *Bull. Seismol. Soc. Am.*, 97(6), 1793–1802, doi:10.1785/0120050211.
- Rice, J. R. (2006), Heating and weakening of faults during earthquake slip, *J. Geophys. Res.*, 111(B5), doi:10.1029/2005JB004006.
- Rice, J. R., and A. L. Ruina (1983), Stability of Steady Frictional Slipping, *J. Appl. Mech.-T. ASME*, 50(2), 343–349.
- Ripperger, J., J.-P. Ampuero, P. M. Mai, and D. Giardini (2007), Earthquake source characteristics from dynamic rupture with constrained stochastic fault stress, *J. Geophys. Res. Solid Earth*, 112(B4), B04311, doi:10.1029/2006JB004515.
- Rockwell, T., C. Loughman, and P. Merifield (1990), Late Quaternary rate of slip along the San Jacinto Fault Zone near Anza, southern California, *J. Geophys. Res. Solid Earth*, 95(B6), 8593–8605, doi:10.1029/JB095iB06p08593.
- Rockwell, T., G. Seitz, T. Dawson, and J. Young (2006), The long record of San Jacinto fault paleoearthquakes at Hog Lake: Implications for regional patterns of strain release in the southern San Andreas fault system, *Seismol. Res. Lett.*, 77 (2), 270.

- Rockwell, T. K., T. E. Dawson, J. Y. Ben-Horin, and G. Seitz (2014), A 21-event, 4,000-year history of surface ruptures in the Anza seismic gap, San Jacinto fault, and implications for long-term earthquake production on a major plate boundary fault, *Pure. Appl. Geophys.*, 172(5), 1143–1165, doi:10.1007/s00024-014-0955-z.
- Ruina, A. (1983), Slip instability and state variable friction laws, *J. Geophys. Res. Solid Earth*, 88(B12), 10,359–10,370, doi:10.1029/JB088iB12p10359.
- Salisbury, J. B., T. K. Rockwell, T. J. Middleton, and K. W. Hudnut (2012), LiDAR and field observations of slip distribution for the most recent surface ruptures along the Central San Jacinto Fault, *Bull. Seismol. Soc. Am.*, 102(2), 598–619, doi:10.1785/0120110068.
- Sammis, C. G., and J. R. Rice (2001), Repeating earthquakes as low-stress-drop events at a border between locked and creeping fault patches, *Bull. Seismol. Soc. Am.*, 91, 532–537, doi:10.1785/0120000075.
- Sanders, C. O. (1990), Earthquake depths and the relation to strain accumulation and stress near strike-slip faults in southern California, *J. Geophys. Res. Solid Earth*, 95(B4), 4751–4762, doi:10.1029/JB095iB04p04751.
- Sanders, C. O., and H. Kanamori (1984), A seismotectonic analysis of the Anza Seismic Gap, San Jacinto Fault Zone, southern California, *J. Geophys. Res. Solid Earth*, 89(B7), 5873–5890, doi:10.1029/JB089iB07p05873.
- Savage, J. C. (2006), Dislocation pileup as a representation of strain accumulation on a strike-slip fault, *J. Geophys. Res.*, 111 (B4), B04,405–14, doi:10.1029/2005JB004021.
- Savage, J. C., and R. O. Burford (1973), Geodetic determination of relative plate motion in central California, *J. Geophys. Res.*, 78 (5), 832–845, doi:10.1029/JB078i005p00832/pdf.

- Scholz, C. H. (1998), Earthquakes and friction laws, *Nature*, 391 (6662), 37–42.
- Shi, Z., and S. M. Day (2013), Rupture dynamics and ground motion from 3-D rough-fault simulations, *J. Geophys. Res. Solid Earth*, 118(3), 1122–1141, doi:10.1002/jgrb.50094.
- Smith-Konter, B. R., D. T. Sandwell, and P. M. Shearer (2011), Locking depths estimated from geodesy and seismology along the San Andreas Fault System: Implications for seismic moment release, *J. Geophys. Res.*, 116 (B6), B06,401, doi:10.1029/2010JB008117.
- Thatcher, W., J. A. Hileman, and T. C. Hanks (1975), Seismic slip distribution along the San Jacinto fault zone, Southern California, and its implications, *Geological Society of America Bulletin*, 86 (8), 1140–1146, doi:10.1130/0016-7606(1975)86<1140:SSDATS>2.0.CO;2.
- Townend, J., and M. D. Zoback (2004), Regional tectonic stress near the San Andreas fault in central and southern California, *Geophys. Res. Lett.*, 31(15), 115S11, doi:10.1029/2003GL018918.
- Tullis, T. (2015), Mechanisms for friction of rock at earthquake slip rates, in *Treatise on Geophysics (Second Edition)*, edited by G. Schubert, second edition ed., pp. 139–159, Elsevier, Oxford, doi:10.1016/B978-0-444-53802-4.00073-7.
- van der Woerd, J., Y. Klinger, K. Sieh, P. Tapponnier, F. J. Ryerson, and A.-S. Meriaux (2006), Long-term slip rate of the southern San Andreas Fault from <sup>10</sup>Be-<sup>26</sup>Al surface exposure dating of an offset alluvial fan, *J. Geophys. Res. Solid Earth*, 111(B4), B04407, doi:10.1029/2004JB003559.
- Wdowinski, S. (2009), Deep creep as a cause for the excess seismicity along the San Jacinto fault, *Nat. Geosci.*, 2(12), 882–885, doi:10.1038/ngeo684.

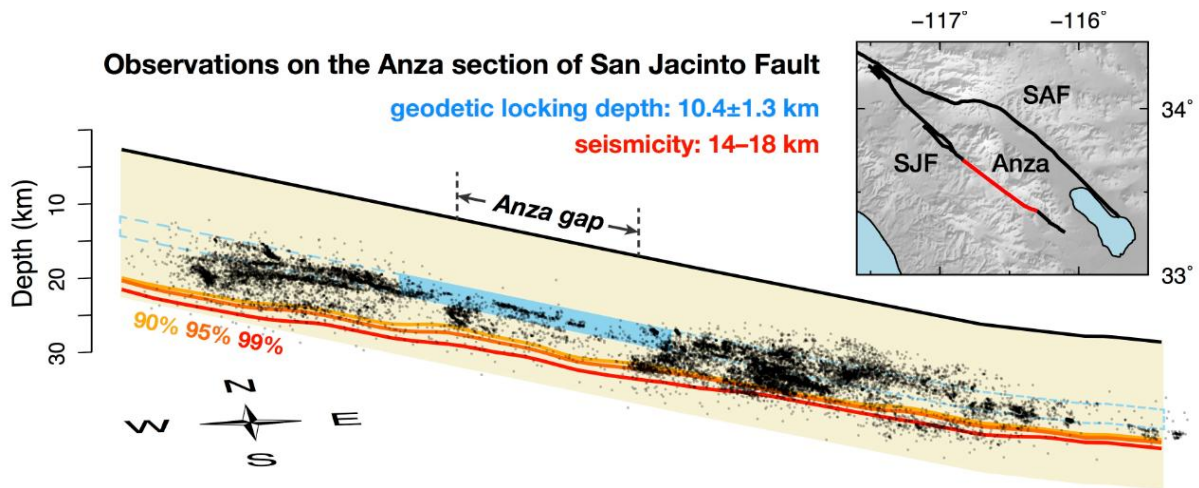


**Figure 1.** Observations from the Anza section of the San Jacinto Fault (SJF) in Southern California. Regional topography (gray) and surface traces (black) of the San Andreas Fault (SAF) and SJF are drawn in the map, with the trace of SFJ near the Anza gap highlighted in red. The fault geometry of the highlighted section (Community Fault Model, *Plesch et al.*, 2007) is visualized in three dimensions, together with seismicity (black dots) that occurs within 3 km of the fault plane between 1981–2011 [*Hauksson et al.*, 2012]. The 90%, 95%, and 99% cutoff depths of seismicity are delineated in yellow, orange, and red, respectively. The  $1\sigma$  uncertainty range of the geodetically-determined locking depth is represented by a blue band [*Lindsey et al.*, 2014].

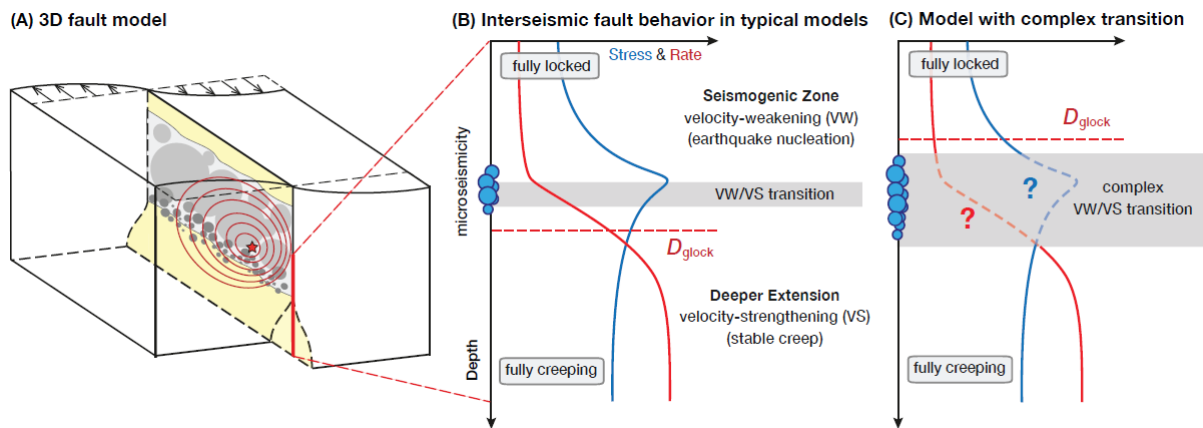


**Figure 2.** Locked-creeping transition on faults in the interseismic period. (A) The conceptual model of a strike-slip fault with the seismogenic zone (SZ, gray), creeping regions (yellow), and fault heterogeneity at transitional depths (gray circles). Earthquakes initiate at the lowermost SZ (red star) and rupture through the region (rupture fronts in red). (B) The locked SZ and deeper creeping fault extension are typically interpreted as having VW and VS frictional properties, respectively. In the interseismic period, the transition between the locked SZ and fully creeping regions occurs over a broad depth range (see red line). The geodetic locking depth,  $D_{\text{glock}}$ , thus lies in the midst of this transition zone, while concentrated stressing is located near the base of the SZ (see blue line) and promotes microseismicity (blue circles) near the relatively sharp VW/VS transition. As a result, geodetic locking depth should be greater than, or comparable to the depths of concentrated seismicity. (C) A complex transition zone may change the relative locations of seismicity and geodetic locking depth.



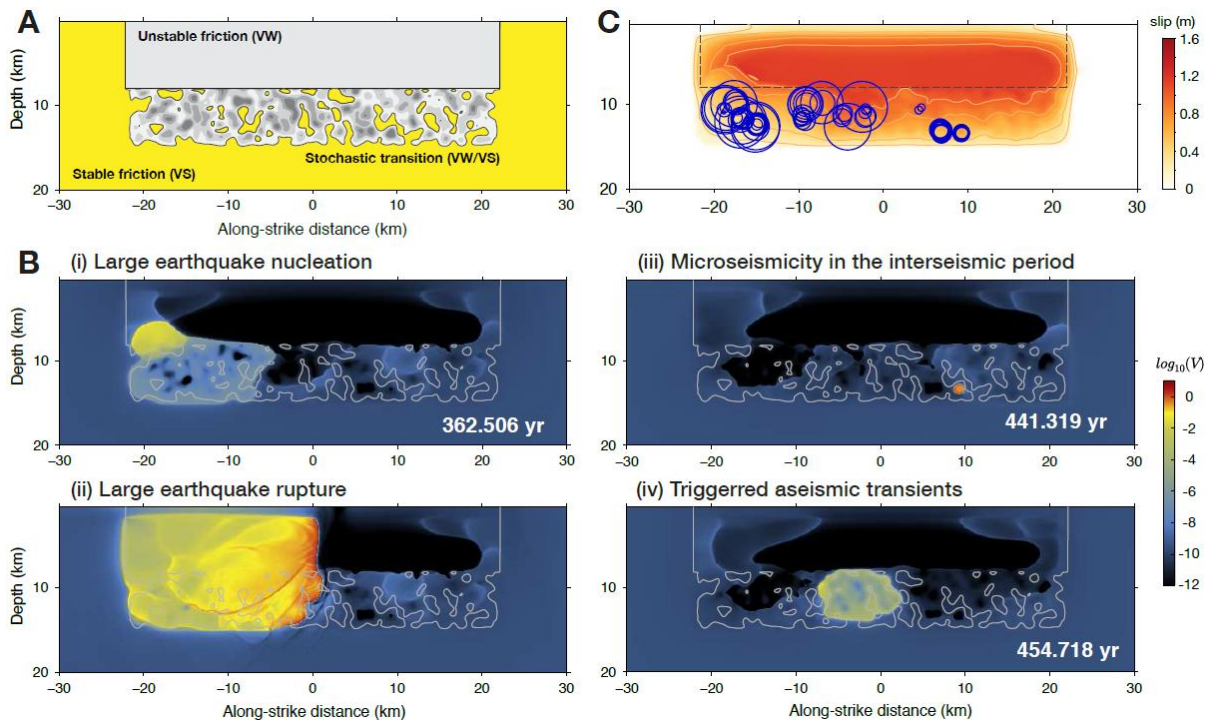


**Figure 3.** A large earthquake and microseismicity in a 3D fault model with heterogeneous frictional properties. (A) In the model, a transition zone with stochastic heterogeneity in frictional properties exists between the shallower VW (gray) and deeper VS (yellow) regions. (B) Different stages in the long-term fault behavior illustrated by snapshots of fault slip rates on a logarithmic scale, including nucleation and rupture of large events, microseismicity, and aseismic transients. (C) Spatial patterns of microseismicity (circles) in the post- and inter-seismic periods of a typical large earthquake (coseismic slip in color). The size of circles is based on a circular crack model [Eshelby, 1957] with the same seismic moment and 3 MPa stress drop.

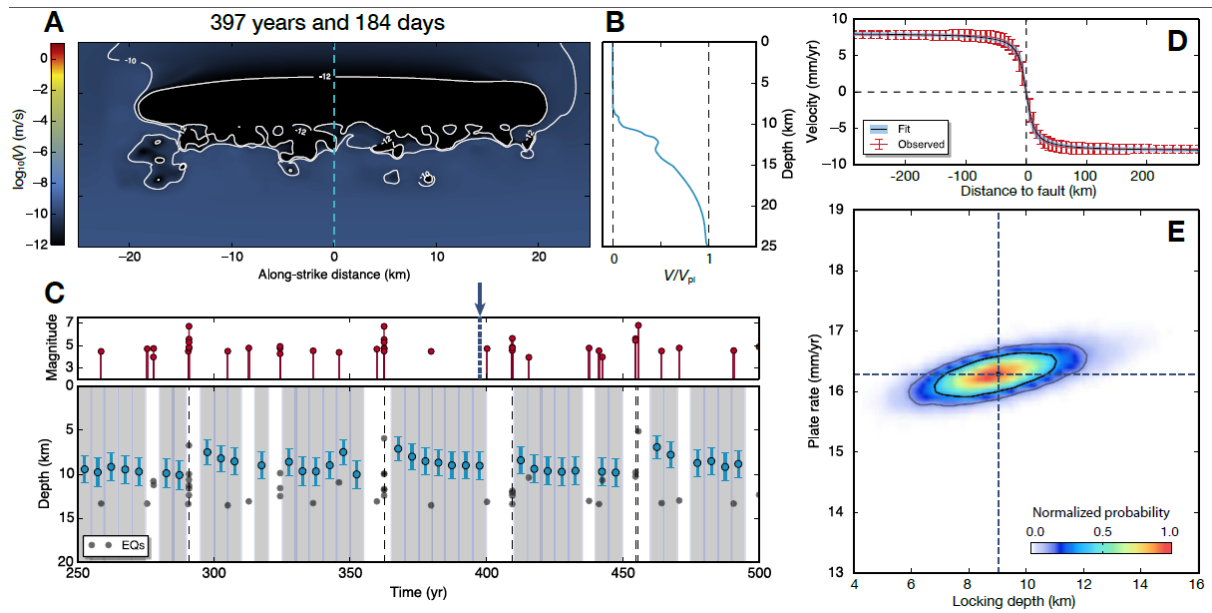


**Figure 4.** Depth extent of seismicity and fault locking in our model. (A) Average slip rates on the fault over 5 years shown on a logarithmic scale. (B) The depth distribution of slip rates along a mid-fault profile shown in (A), with the shallower fault areas ( $< 5$  km) assumed to be fully locked. (C) (Top panel) moment magnitudes of seismicity that occurs over the period of several large events. The blue arrow points to the time window we consider for the analysis in (D) and (E). (Bottom panel) time evolution of depths of seismicity (black circles) and the inferred geodetic locking depths (blue circles with  $1\sigma$  error bars) in respective time windows (gray bands). (D) The fault-normal profile of synthetic along-strike surface velocity (red line) with assumed observational errors (red error bars). The  $2\sigma$  range of posterior data fit is shown in blue and the best fit in black. (E) Normalized joint probability density distribution for the geodetic locking depth and plate loading rate.  $1\sigma$  (68%) and  $2\sigma$  (95%) credible regions are encircled by thick and thin black lines. The dashed lines indicate the posterior mean values.